Spray-Coated, Magnetically Connectable Free-Standing Epidermal Electrodes for High Quality Biopotential Recordings

Andrea Spanu,* Mohammad Taki, Giulia Baldazzi, Antonello Mascia, Riccardo Pietrabissa, Danilo Pani, Piero Cosseddu, and Annalisa Bonfiglio*

Acquiring biopotentials from the surface of the body is a common procedure both in the clinical practice and in non-clinical applications as sport and human-machine interfaces. To avoid bulky recording systems and to allow optimal long-term measurements, several tattooable solutions were recently developed, aiming at high-quality and imperceptible electrodes. However, a seamless connection with epidermal electrodes still represents one of the biggest challenges in this field. In this paper, we propose a simple and efficient approach for the fabrication of free-standing epidermal electrodes that can be contacted using small magnetic connectors, thus directly tackling this issue. The proposed electrodes are fabricated using a conductive ink based on poly(3,4-ethylenedioxythiophene) polystyrene sulfonate (PEDOT:PSS) deposited by spray coating, and can be easily contacted using magnetic connectors without disrupting their conformability, thanks to the presence of ferrite nanoparticles integrated within the thin film itself. These electrodes have been successfully employed for the detection of different biopotentials, namely electrocardiogram, electromyogram and electro-oculogram, demonstrating excellent performances for the detection of biosignals from delicate body parts, such as the face, thus demonstrating the effectiveness of the approach for the development of a new generation of magnetically connectable epidermal electrodes for critical biopotentials monitoring.

1. Introduction

The advantages of using ultrathin epidermal electrodes for the detection of biopotentials from the surface of the skin are nowadays widely recognized. In fact, the technological advancements that the field of epidermal electronics has undergone in the past decade have lately led to a plethora of different interesting approaches and solutions. In particular, several types of ultrathin dry electrodes and devices have been introduced in the biomedical field and used for several applications, such as biopotential recording and biochemical sensing,[1–6] as well as for pressure/temperature sensing,[7–9] not only for clinical applications but also for human-machine interfaces and even gaming.[10,11] Nonetheless, one of the most explored applications, probably the one that mostly benefits from the epidermal approach, still remains the recording of bio-potentials from the surface of the skin. In fact, despite being the most used solution, commercial pre-gelled Ag/AgCl electrodes are characterized by undeniable limitations, such as the possible induction of skin irritation, due to the presence of a sticky, Cl$^-$-loaded electrolytic gel, and a gradual worsening of the performance over time due to the progressive drying of the gel caused by the evaporation of the water component.[12,13] In the attempt of overcoming those limitations, several epidermal solutions have been proposed for the monitoring of biosignals such as electrocardiography (ECG),[14] electromyography (EMG),[15,16] electroencephalography (EEG),[17] and electrooculography (EOG).[18] Several fabrication approaches have been proposed in the recent past, ranging from Parylene C ultrathin electrodes to ultrathin microstructured meshed electrodes,[19] metallic nanowire-based electrodes,[20] and conductive polymer-based temporary tattoos.[21] In particular, following the increasing interest that the latter approach has generated, epidermal and textile electrodes based on the conductive polymer poly(3,4-ethylenedioxythiophene) polystyrene sulfonate (PEDOT:PSS) have gained considerable attention due to their advantages such as the potential use of low-cost fabrication methods, very good biocompatibility, and optimized skin-electrode interface. These electrodes have been

A. Spanu, R. Pietrabissa, A. Bonfiglio
University School for Advanced Studies (IUSS)
Piazza della Vittoria 15, 27100 Pavia, Italy
E-mail: andrea.spanu@iusspavia.it; annalisa@diee.unica.it

M. Taki, G. Baldazzi, A. Mascia, D. Pani, P. Cosseddu, A. Bonfiglio
Department of Electrical and Electronic Engineering
University of Cagliari
via Marengo, 09123 Cagliari, Italy

M. Taki
Department of Electrical & Electronics Engineering
Lebanese International University
146404 Beirut, Lebanon

The ORCID identification number(s) for the author(s) of this article can be found under https://doi.org/10.1002/adem.202302195.

lately proposed for the acquisition of ECG, EMG, EOG, and EEG[22–29] signals but, unfortunately, the limitations stemming from their difficult interfacing with conventional connectors, which are rigid and bulky, strongly limited the exploitation of this approach. Recently, this group proposed an alternative solution aimed at overcoming this limitation, i.e., a PEDOT:PSS-based free-standing film with an embedded ferrimagnetic component.[30] The idea behind that work was to eliminate the necessity of a connection part within the film itself (which has to be thicker than the rest of the film and usually destroys its conformity to the skin). This result was accomplished by loading the film with a ferrimagnetic material enabling the electrical contact with the external readout electronics by using a simple magnetic termination on the cable, without affecting the uniformity of the electrode. Although presenting several merits, the approach was limited by a process that was not suitable for large-area fabrication, and from a non-optimal uniformity of the ferrimagnetic material within the film.

In this article, we propose an innovative, up-scalable and more convenient approach for the development of optimized conductive and ferrimagnetic functional films suitable for biopotentials detection. In particular, differently from the afore-mentioned approach (which required an additional silver layer to ensure an effective electrical contact between the magnetic connector and the epidermal film), this solution allows a very good control of the uniformity of the film and ensures an optimal contact between the film and the external magnetic connector that in this way can be easily attached/detached from the measuring electrode without perturbing the quality of the conformal contact between the skin and the electronic tattoo. In synthesis, we have developed a method for obtaining a new type of epidermal electrodes consisting in fully spray-coated films based on PEDOT:PSS as conducting polymer and inexpensive ferrite powder as ferrimagnetic material, which can be easily transferred to the skin and directly contacted with magnetic connectors.

Differently from other approaches such as spin coating, spray coating offers several advantages, like an easier patternability, a much faster and uniform deposition over larger areas and, in the specific case of conductive/ferrimagnetic free-standing films for biopotential recordings, a better distribution of the ferrimagnetic powder, which leads to higher magnetic forces of attraction at lower thicknesses, while preserving the optimal value of the skin-electrode impedance. Spray-coating has already been used to deposit PEDOT:PSS for the fabrication of thin films and electrodes,[31,32] functionalized fabrics,[33] solar cells,[34] and organic electronics devices, sensors and transistors,[35–37] while, recently, an aerosol jet printing technique has been proposed for the patterning of superparamagnetic features, thus confirming the possibility of conveniently depositing magnetite nanoparticles in an efficient way.[38] However, the jet printing technique is not suitable for large-area applications, being more convenient for the development of high-resolution features on small areas. Interestingly, the approach presented in this work is, to our knowledge, the first example of an up-scalable, large area method for the fabrication of free-standing PEDOT:PSS/PVA-based epidermal electrodes that ensure both surface and vertical conductivity and can be contacted from the back-side using magnetic connectors, thanks to a combination of (biocompatible) materials and a low-cost, large-area spray coating layer-by-layer technique,

here employed to obtain functional free-standing films (rather than as a method to simply transfer a certain material onto a substrate). In fact, none of the solutions already present in the literature are able to provide a way to obtain free-standing and isotropically conductive films, due to the presence of a (non-conductive) substrate or backside material. For example, PEDOT:PSS films/electrodes based on tattoo paper, once laminated on the skin present a thin layer of ethyl cellulose, and an analogous problem (i.e., the presence of a non-conductive back material) affects Parylene C-based ultrathin electrodes and all the other non-free-standing approaches. Our approach, on the contrary, allows in detaching the film from the carrier without compromising its vertical conductivity, while at the same time giving the possibility of finely tuning the thickness and the magnetic force of attraction.

The mechanical requirements of the electrodes manufactured using the technologies and materials previously outlined stem from the need to 1) maximize the contact surface between the measurement device and the skin and 2) maintain a constant contact surface following the application of the measurement device, regardless of skin movements. The first point depends on the flexibility and radius of curvature that the device can assume to adapt to the skin's surface. In fact, the capability of thin films to conform to a certain surface depends on their ability to withstand bending around small curvature radii, which in turn depends on the superficial residual stress induced by the deformation. According to the Stoney formula, two important parameters that affect the superficial stress of a thin film deposited on a flexible substrate are the film thickness and its Young's modulus (which for PEDOT:PSS/PVA films lies in the range of 1–2 GPa[39]). In particular, the lower the Young's modulus and the smaller the thickness, the lower will be the superficial stress, thus allowing the film to resist to higher deformations. The skin macroscopic roughness, however, varies considerably depending on the body area, hydration, age, and other individual characteristics,[40,41] and is on the order of tens of microns,[42–44] which is considerably larger than the thickness of the proposed electrodes. As shown in **Figure 1** and **2**, the device adheres well, perfectly reproducing the roughness of the underlying skin. Therefore, the flexibility and radius of curvature appear suitable for maximizing the contact surface.

The second point depends on the ratio between the contact force (between the device and the skin), which is electrostatic in nature and thus weak, and the shear stress that arises due to skin dilation or compression, which, to maintain perfect adhesion, must cause the device to expand or compress itself. This phenomenon is certainly dependent on the maximum shear force between the device and the skin before detachment, the elasticity modulus of the device, and its thickness. In a future study, this aspect, which is crucial for measurement reliability, will be thoroughly investigated.

In the following, we will report that these epidermal films showed remarkable performances in terms of their capability of detecting different types of biopotentials, namely ECG, EMG, and EOG, thus making the proposed technique a very convenient approach for the high-volume fabrication of high-performing epidermal electrodes for biopotentials acquisition.
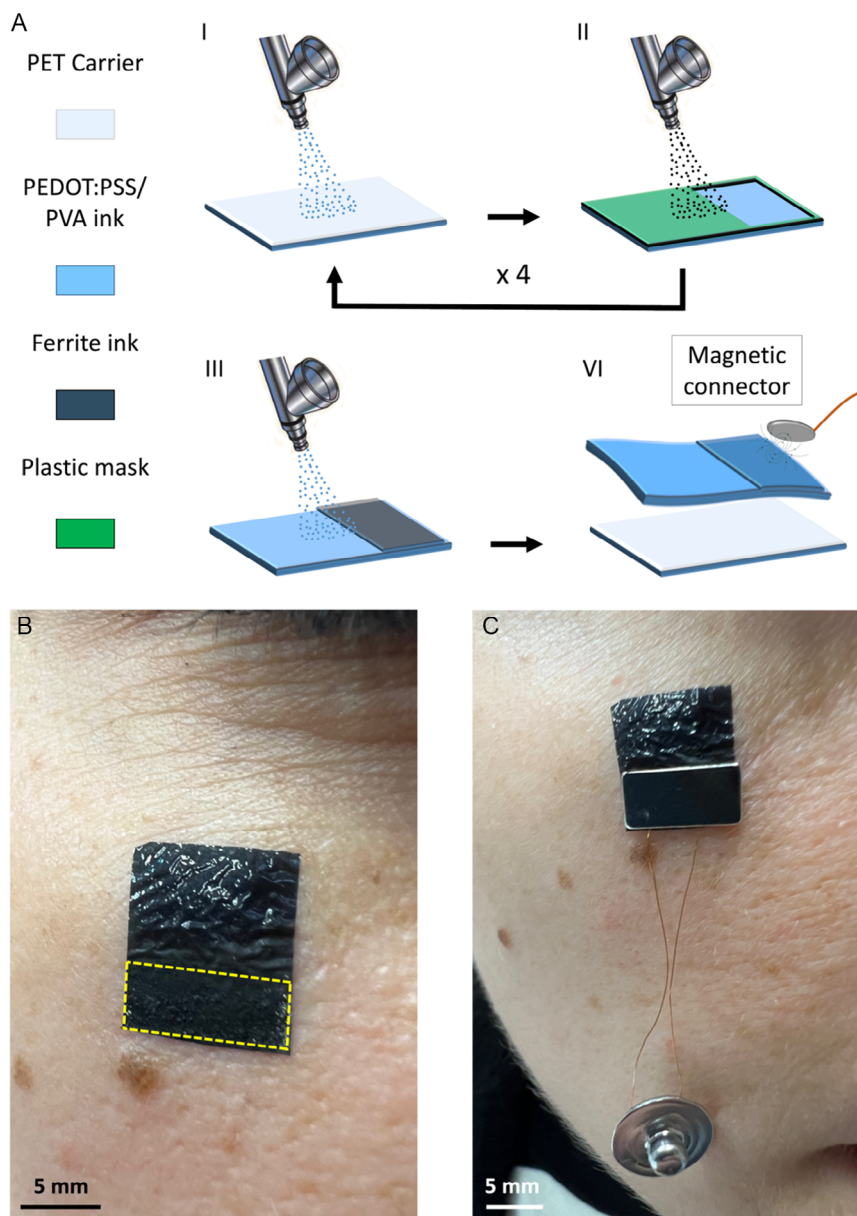
Figure 1. A) Fabrication process of the conductive ferrimagnetic film for biopotential recordings. I) A first conductive layer is spray-coated onto a PET carrier, followed by a ferrite layer, which is spray coated onto the desired portion of the film through a plastic mask (II). The process is repeated four times. After the deposition of a final conductive layer (III) the film can be easily detached from the carrier (VI). B) A ferrimagnetic/conductive electrode placed on the subject's cheekbone (the yellow dotted line indicates the ferrimagnetic/conductive part, otherwise indistinguishable from the rest of the electrode). C) The same electrode contacted with a custom magnetic connector consisting in a 5 mm × 10 mm conductive Nd magnet connected to a snap contact through thin insulated copper wires.

2. Results and Discussion

2.1. Electrodes Fabrication and Characterization

The freestanding films were fabricated using a layer-by-layer process. As a first step, a PEDOT:PSS solution blended with poly (vinyl alcohol) (PVA) was deposited by spray coating on a 15 × 15 cm poly(ethylene terephthalate) (PET) substrate, which acts as the carrier. The pressure of the compressor was fixed at 4 bar and the distance between the samples and the airbrush was kept at 15 cm. The volume of the conductive ink solution deposited for each layer was 1 mL. After the first deposition, the samples were baked at 70 °C for 20 min in a standard convection oven to ensure the complete evaporation of the solvent. As a second step, 1 mL of a ferrite dispersion in isopropanol was deposited on the dry conductive layer. The ferrite was selectively deposited over a specific portion of the film through a laser-patterned PET mask, in order to obtain a two-part electrode: a
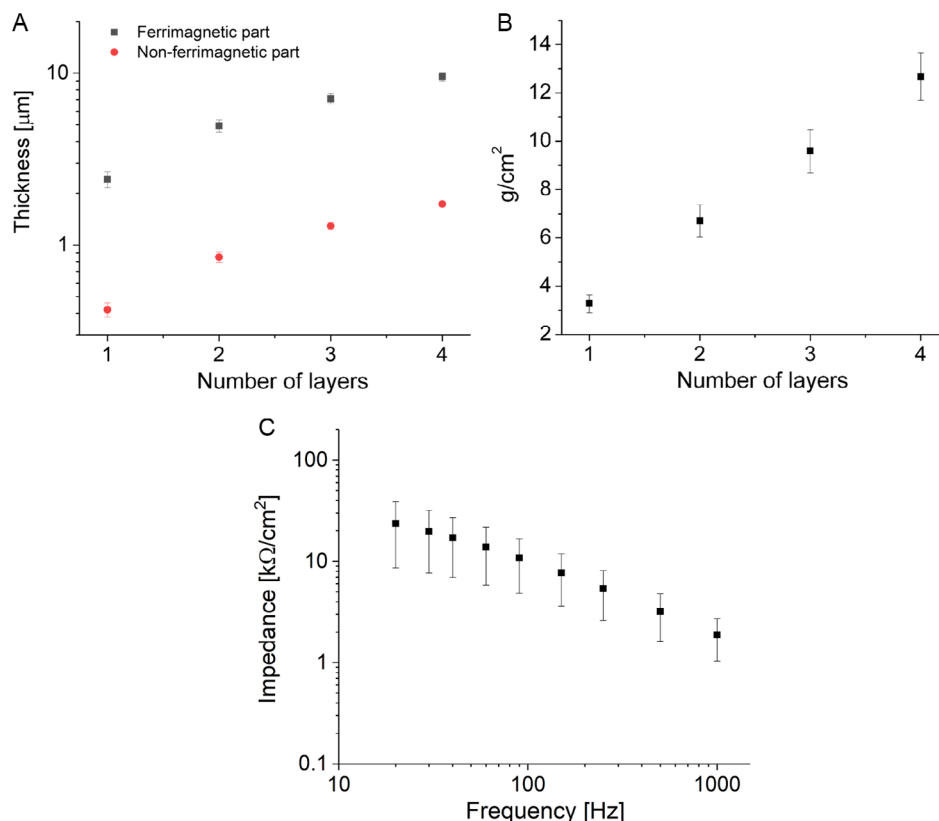
**ADVANCED
SCIENCE NEWS**

www.advancedsciencenews.com

**ADVANCED
ENGINEERING
MATERIALS**

www.aem-journal.com

Figure 2. A) Characterization of the thickness of the film (both the conductive and the ferrimagnetic/conductive part). B) Characterization of the ability of the electrode to withstand a mechanical load. C) Characterization of the skin/electrode impedance for the final electrodes ($n = 10$).

thin conductive part for an optimal skin interfacing, and a thicker portion, both conductive and ferrimagnetic, which can be used for the magnetic connection. After the deposition of the ferrimagnetic solution with isopropanol, the samples were baked in an oven at 50 °C for 5 min to ensure the complete evaporation of the isopropanol.

The whole process was repeated four times (thus four PEDOT: PSS/PVA layers and four ferrite layers). As a final step, a further layer of PEDOT:PSS/PVA was deposited using the same technique. All the electrodes characterized in this article were cut out from the substrate with the same planar size, namely 10 mm × 15 mm (10 mm × 10 mm for the thin conductive part, and 10 mm × 5 mm for the ferrimagnetic/conductive part). The film can be eventually peeled-off from the PET carrier and placed on a piece of paper using few droplets of deionized water, from which it can be conveniently transferred onto the skin. The whole fabrication process is shown in Figure 1A, while in Figure 1B,C, respectively, a conductive/ferrimagnetic electrode after the lamination on the skin and after the connection with a magnetic connector is shown.

The characterization of the thickness and the magnetic force of interaction of the films are reported in Figure 2A,B respectively. Figure S1, Supporting Information, shows a comparison of the magnetic properties of spray coated and spin coated films,[30] highlighting the substantial improvement of the process.

For the final four-layer electrode, the average conductivity of the thin conductive part was 9.0 ± 0.2 S cm^{-1}, whereas that of the conductive/ferromagnetic part was 5.6 ± 0.4 S cm^{-1}. In Figure 2C the characterization of the skin/electrode impedance is also reported. The obtained values are in line with those of other epidermal electrodes for biopotentials monitoring.[45]

The spray-coating technique allowed obtaining a good distribution of both the PEDOT:PSS/PVA-based ink and the ferrite suspension over the carrier, which lead to a very good reproducibility of the process. In Figure S2, Supporting Information, the optical and atomic force microscopy (AFM) characterization of the film is shown. It is possible to observe that the roughness of the film surface is significantly different in the two portions of the electrode, being the rms roughness equal to 6 nm in the purely conductive portion and 21 nm in the magnetic-conductive area. **Figure 3**A,B show the SEM and XRD characterization of both parts of the film, respectively. The peaks corresponding to ferrite (Fe kalfa and Fe kbeta) are much more pronounced in the sample including the ferrimagnetic part while only Fe kalfa is scarcely visible in the spectrum taken on the conductive portion of the film, probably due to a slight contamination of this portion of the film during the deposition process. Figure 3C shows the cross section of the PEDOT:PSS/PVA portion of the film, and Figure 3D shows the cross section of the PEDOT:PSS/PVA + Ferrite part, where the effect of the layer-by-layer deposition can be clearly appreciated.
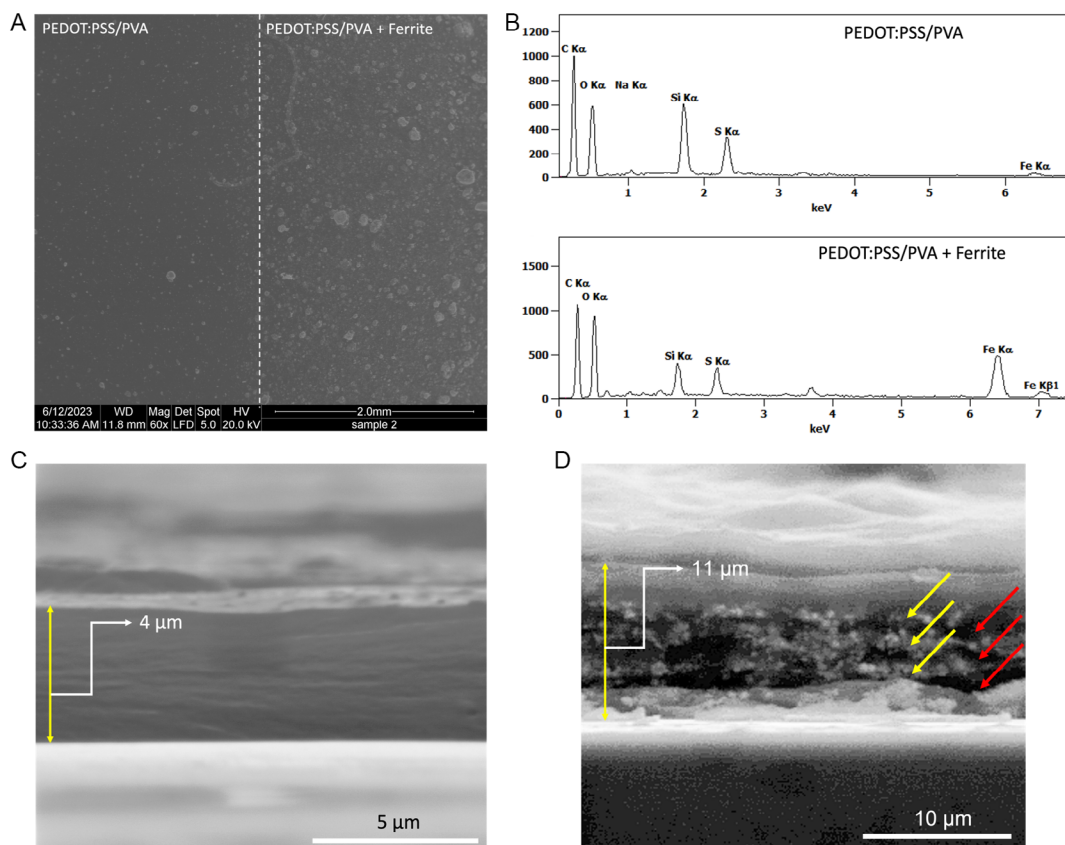
Figure 3. A) SEM image of the surface of a ferrimagnetic/conductive electrode. B) Characterization of both the PEDOT:PSS/PVA and the PEDOT:PSS/PVA + Ferrite part (obtained using a FEI Quanta 200 SEM equipped with an energy dispersive spectrometer – EDS - for X-Ray microanalisys). C and D) Cross section of the PEDOT:PSS/PVA and the PEDOT:PSS/PVA + Ferrite parts, respectively. In (D) it is noticeable the effect of the layer-by-layer fabrication process (yellow arrows: ferrite layer; red arrows: PEDOT/PVA layer).

Interestingly, the ferrite employed in this work is simply a commercial low-cost product (a complete SEM and PXRD characterization is shown in Figure S3, Supporting Information, while in Figure S4, Supporting Information, an optical image of the surface highlights the improvements over the spin-coated version[30]). This deliberate choice highlights the effectiveness of the approach, regardless of the type of magnetic/ferrimagnetic/ferromagnetic material employed. Nevertheless, the overall performance of the film can be of course improved and specifically tailored with respect to the targeted application by choosing the magnetic/ferrimagnetic/ferromagnetic material and the particles size and/or possible functionalization.

2.2. Biopotential Recordings

The proposed conductive-ferrimagnetic electrodes were characterized and compared with pre-gelled Ag/AgCl commercial ones of similar size. The acquisitions were done at the same time, placing the electrodes in symmetrical or very similar (but not identical) positions. This obviously slightly affects the comparison in terms of morphology of the acquired signal. Nevertheless, the correlation and consistency between the signals detected by the different electrodes was very clear both in time and frequency domains.

2.2.1. ECG Signals

High-quality ECG acquisitions were performed by ferrimagnetic epidermal electrodes at rest. We noticed that, despite ferrimagnetic electrode ECG suffered from baseline wander more than Ag/AgCl one (root mean square (RMS) = 0.239 mV for ferrimagnetic electrodes, RMS = 0.032 mV for Ag/AgCl ones), its baseline wandering was comparable to that of other recent epidermal electrodes.[30,45] Furthermore, despite relying on a dissimilar electrode positioning leading to slightly different waveform morphologies (as showed in **Figure 4**A), ECG signals acquired by the two types of electrodes exhibited a good correlation ($\rho = 0.90$, see Figure 4B), with consistent RR interval estimations (800 ± 46 ms for both ferrimagnetic and Ag/AgCl electrodes). The similarity between the Ag/AgCl and ferrimagnetic ECG acquisitions was also assessed in the frequency domain (see Figure 4C), where the typical spectral contributions present in the ECG waveforms[46] can be appreciated.

2.2.2. Results on EMG Signals

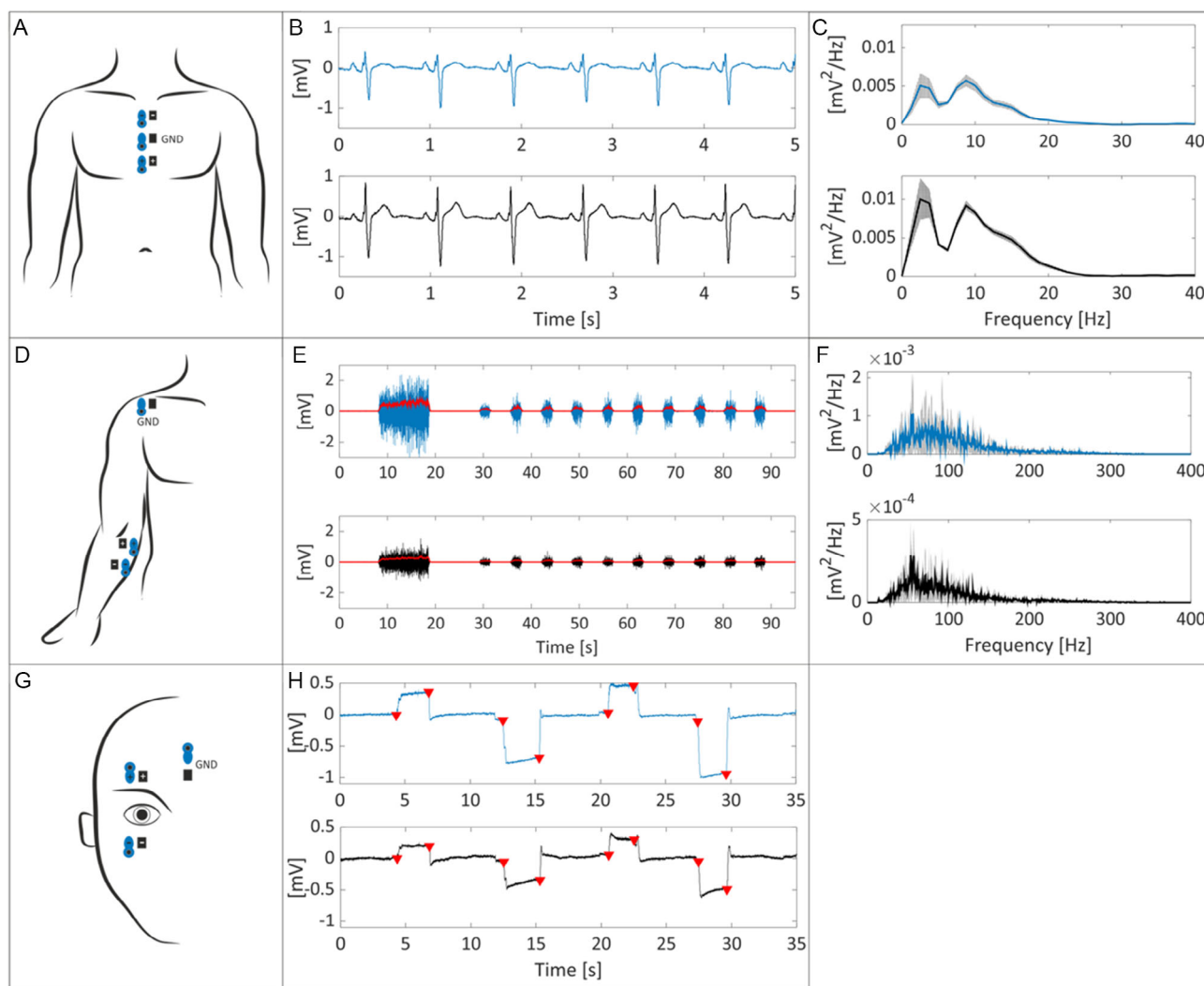Surface EMG signal acquisition was performed on a healthy volunteer by placing the two pairs of measuring electrodes

Figure 4. Electrode positioning and bio-potentials acquired during the different experimental sessions. A) Electrode positioning adopted for ECG recording by using Ag/AgCl (in blue) and ferrimagnetic electrodes (in black). B) High-pass filtered ECG signals (with cut-off frequency of 0.67 Hz) acquired by Ag/AgCl (top) and ferrimagnetic electrodes (bottom). C) One-sided power spectral density (PSD) for Ag/AgCl (top) and ferrimagnetic (bottom) ECG recordings; PSDs are computed on each beat after Hamming windowing, and then reported as mean trend (black line) $\pm$ the standard deviation (grey shading). D) Electrode positioning adopted for surface EMG recording by using Ag/AgCl (in blue) and ferrimagnetic electrodes (in black). E) Band-pass filtered EMG signals (between 20 and 400 Hz) recorded by Ag/AgCl (top) and ferrimagnetic electrodes (bottom), with the corresponding envelopes (in red). F) PSD for Ag/AgCl (top) and ferrimagnetic (bottom) EMG recordings; PSDs were computed on each post-MVC muscular activation after Hamming windowing, and then reported as mean trend (black line) $\pm$ the standard deviation (grey shading). G) Electrode positioning adopted for EOG recording by using Ag/AgCl (in blue) and ferrimagnetic electrodes (in black). H) EOG signals acquired by Ag/AgCl (top) and ferrimagnetic electrodes (bottom) with the onsets detected for each saccade (red markers).

(namely the ferrimagnetic electrodes and disposable gelled Ag/AgCl ones) on the flexor carpi ulnaris muscle, while the ground electrode was positioned on the acromion (see Figure 4D). During the recording, the volunteer was asked to repeatedly squeeze a hand dynamometer, while monitoring the force exerted during the measurement. As for the ECG signals, EMG acquisition by ferrimagnetic tattoo electrodes was more affected by baseline wandering than Ag/AgCl one (RMS = 1.117 mV for epidermal electrodes, RMS = 0.562 mV for Ag/AgCl ones), but again this aspect did not influence the overall quality of the measurement, which resulted consistently

comparable to that of the gold standard counterpart. We found that low-frequency noise in both Ag/AgCl and ferrimagnetic signals were lower than those reported in ref. [47], where mean RMS noise values were reported equal to 5.9 and 2.3 mV for textile and Ag/AgCl electrodes, respectively, despite considering a different muscle. As can be seen in Figure 4E, the morphologies of the recorded EMG, as well as their envelopes, showed high similarity ($\rho = 0.99$). Remarkably, the similarity appreciated in the time domain was also obtained in the frequency domain (see Figure 4F), even though some amplitude differences can be observed probably due to electrodes positioning.
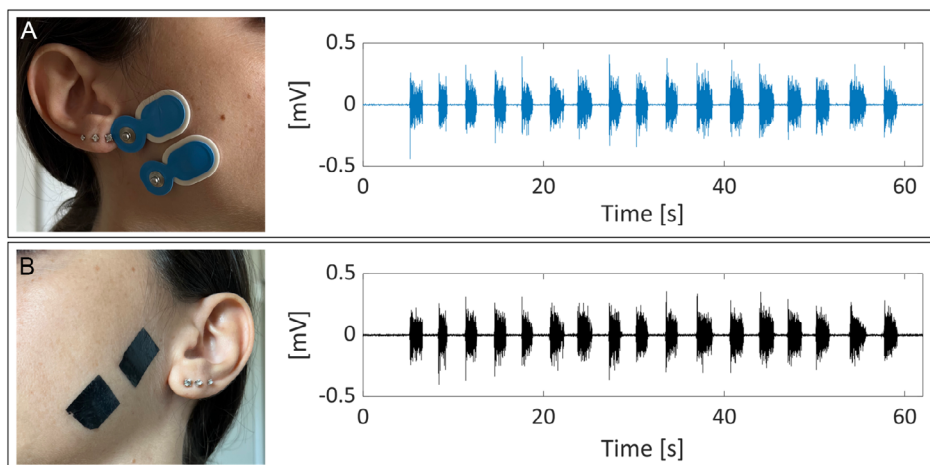
ADVANCED
SCIENCE NEWS
www.advancedsciencenews.com

ADVANCED
ENGINEERING
MATERIALS
www.aem-journal.com

Figure 5. Electrodes positioning (A) Ag/AgCl electrodes and B) ferrimagnetic electrodes) and EMG signals acquired during multiple repetitions of jaw clenching. The EMG signals were band-pass filtered between 20 and 400 Hz.

Furthermore, by considering the estimation of the muscular activation intervals, post-MVC (maximum voluntary contraction) activation time was 2.1 ± 0.1 s for Ag/AgCl, and 2.2 ± 0.1 s for the epidermal electrodes. These values were comparable and consistent with the 2-s long voluntary contractions required by the acquisition protocol, despite an overestimation of the average activation interval of about 57 ms was observed in ferrimagnetic EMG signals. Anyway, this latter value, which is much lower than that reported in ref. [47] reflects an average overestimation of about 3% with respect to the actual duration of the corresponding contraction (absolute error: -0.06 ± 0.05 s; relative error: $-3 \pm 3\%$).

Finally, as a further analysis, ferrimagnetic electrodes were compared to Ag/AgCl ones in surface EMG signal acquisition during jaw clenching, which exploits a challenging electrode positioning (see **Figure 5**A). In this case, the Ag/AgCl electrodes were placed on the right masseter muscle, while the ferrimagnetic ones on the left masseter. As can be clearly seen from Figure 5B, also in this electrode configuration, surface EMGs are comparable and easily detectable in both acquisitions.

2.2.3. Results on EOG Signals

EOG signals were recorded according to a saccade-fixation protocol involving only vertical movements. Also in this case, signal morphologies were highly correlated ($\rho = 0.99$), as can be also appreciated by visual inspection of Figure 4H. Moreover, the timings estimated for the onset of each saccade were quite comparable, with slightly earlier detections of saccadic movement onset occurring in case of ferrimagnetic epidermal electrodes (absolute error: -3 ± 3 ms).

3. Conclusion

In this article, a convenient combination of materials and large-area process for the fabrication of epidermal conductive/ferrimagnetic electrodes allowing an optimal quality of the signal

and a reliable interface with both the skin and the measurement instrumentation was presented. In particular, the proposed electrodes were obtained using a simple and reproducible spray-coating technique that allowed to obtain free-standing, functional films based on PEDOT:PSS/PVA ink and ferrite powder, exhibiting three-axial conductivity and suitable for high-fidelity biopotentials detection. These epidermal electrodes can be contacted using simple magnetic connectors and allow a very comfortable placement for the patient, even in areas (like the face) that are normally quite critical, and where commercial Ag/AgCl electrodes, besides being bulky and impractical, may cause severe irritation. The preliminary validation of the electrodes showed very good performance in the detection of ECG, EMG, and EOG biosignals, thus demonstrating the feasibility of the proposed fabrication approach and its suitability for biomedical applications, paving the way to a future generation of truly imperceptible electrodes and devices that can be conveniently exploited both in clinical and non-clinical scenarios. It is worth pointing out here that the applications of such magnetic connectors could pose potential safety risks, and their use must be carefully evaluated in subjects with pacemakers or implantable cardioverter defibrillators.[48]

4. Experimental Section

Materials: The conductive ink was prepared by a mixing two parts: a conductive part based on the organic material PEDOT:PSS and a solution of a nonconductive material, i.e., PVA. The presence of PVA allowed to easily remove the film from the carrier substrate, thanks to its film-forming properties.[49] The conductive ink was prepared by mixing 70% v/v of PEDOT:PSS (Clevios PH1000, by Heraeus, Germany) with 30% v/v of ethylene glycol (by Merck KGaA, United States), followed by the addition of 1% (in volume of the previous blend) of 3-Glycidyloxypropyl trimethoxysilane-GOPS (by Merck KGaA, United States), which was used as reticulant agent. The PVA solution was previously prepared by dissolving the PVA (molecular weight: 205 kg mol^{-1}) in de-ionized water (10% in weight). The conductive ink was then blended with a 4% of this PVA solution. The ferrite ink was prepared as a simple ferrite powder suspension (commercial Fe_3O_4, the SEM and PXRD characterization of the powder can be

**ADVANCED
SCIENCE NEWS**

www.advancedsciencenews.com

**ADVANCED
ENGINEERING
MATERIALS**

www.aem-journal.com

found, Figure S2, Supporting Information) in isopropanol (10% of ferrite in weight).

Magnetic Force Characterization: To measure the magnetic force of attraction between the conductive/ferrimagnetic portion of the film and the magnetic connector, a commercial dynamometer (FCA-DS2-50N by IMADA, United States) mounted on a vertical motorized stand (MX2 by IMADA, United States) was employed. In this setup, the indenter, where a magnet (a circular N52 neodymium magnet with an area of $1 cm^2$) was glued to its end, was slowly moved away from the surface of the film (after being placed in contact with the film itself) and the force of attraction is recorded as the force measured right before the magnets detaches from the film. The attraction between the film and the magnet is expressed in $g cm^{-2}$ by simply converting it from $N cm^{-2}$, as previously reported in ref. [30].

Film Conductivity Characterization: The conductivity of the film has been separately characterized for both the conductive and the conductive/ferrimagnetic part. By using a 4284 A LCR-meter (by Agilent, United States) the resistances of both parts were measured using a four-probe approach. The probes were placed on either side of the film, thus ensuring the existence of the vertical conductivity in addition to the planar conductivity on both sides.

Film Thickness and Surface Morphology Characterization: The thickness of both the conductive and the ferrimagnetic-conductive portions of the films were evaluated using a profilometer (Dektak XT by Bruker, United States). Atomic force microscopy measurements were obtained by means of a SPM SOLVER PRO by NT-MDT in semi-contact mode using NT-MDT NSG01 tips.

Skin-Electrode Impedance Characterization: The skin-electrode impedance of the films has been measured by using the 4284 A LCR-meter (by Agilent, United States) against the Ag/AgCl commercial pre-gelled electrode. The impedance was characterized in the range of frequency 20 Hz–1 kHz.

Biopotentials Acquisition and Performance Evaluation: Different kinds of bio-signal were acquired on healthy volunteers simultaneously by the proposed epidermal electrodes and by disposable gelled Ag/AgCl electrodes (BlueSensor N by Ambu, Denmark), and their characteristics were assessed and compared off-line. All signal processing and quantitative analyses were carried out by using MATLAB R2022a (The MathWorks Inc., USA).

Specifically, an ECG signal, an EMG signal, and an EOG signal were acquired by the two electrode types using the BIOPAC MP36 data acquisition system (BIOPAC Systems Inc., USA) with a sampling rate of 2000 Hz. The electrodes were contacted using a custom connector consisting in a small conductive N52 neodymium magnet connected through a copper wire with a diameter of 30 μm to a snap contact. The experimental protocol was carried out following the principles outlined in the Helsinki Declaration of 1975, as revised in 2000. All participants have signed an informed consent.

ECG Signal Acquisition and Quality Evaluation: ECG signals were acquired in resting state by placing a pair of measuring electrodes on the torso, close to the sternum, and the ground electrode in the middle. As previously stated and as shown in Figure 4A, disposable Ag/AgCl electrodes were positioned beside the ferrimagnetic ones, thus resulting in a slightly different ECG lead recording. The performance of the electrodes in ECG recording was quantified and compared to that offered by gelled Ag/AgCl electrodes in terms of RR interval estimation, signal similarity, and baseline wandering amount. In this regard, 30-s long ECG signals acquired by both epidermal and Ag/AgCl electrodes were high-pass filtered by a bidirectional 2nd-order IIR Butterworth filter with cut-off frequency of 0.67 Hz, according to Kligfield et al.[50] in order to suppress low-frequency noises. Then, by using a state-of-the-art QRS detection algorithm,[51] all R peaks were accurately identified in each ECG signal and used to extract the instantaneous RR intervals. RR intervals were further considered for the ECG quality evaluation, because of their relevance in heart rate variability studies and arrhythmias detection. Then, the ECGs similarity was estimated by computing the normalized Pearson's correlation coefficient (ρ) on the full-length, high-pass filtered ECG signals. Conversely, baseline wandering noise entity was evaluated by considering the RMS value of all ECG signal contributions below 0.67 Hz.

EMG Signal Acquisition and Quality Evaluation: The comparative analysis between the proposed electrodes and the Ag/AgCl ones was carried out by considering the similitude of the recorded EMG signals, the consistency of the detected onset and end of each muscular activation epoch between the two recordings, and the entity of the low-frequency noise. The acquisition protocol involved a 10 s long MVC with clench force of $290.0 \pm 65.5 N$, followed by 10 s of rest and ten repetitions of 2 s long voluntary contractions followed by as many relaxations, as in ref. [47], with clench force of $50.1 \pm 66.9 N$. For the analyses, EMG signals were band-pass filtered by bidirectional 2nd-order IIR Butterworth filters with cut-off frequencies of 20 and 400 Hz.[52] Then, each EMG envelope was estimated by computing the RMS on a 200 ms long sliding window. To assess the signal similarity, the normalized Pearson's correlation coefficient ρ was computed between the full-length envelopes obtained by the two electrode types. Then, on each envelope, muscular activations were identified as those signal portions exceeding the 10% of the MVC, excluding the MVC activation. Finally, low-frequency noise was considered as the signal components below 20 Hz affecting the EMG acquisitions. As such, it was derived as the residual signal obtained by subtracting the high-pass filtered EMG from the corresponding raw signal, and quantified by computing its RMS.

EOG Signal Acquisition and Quality Evaluation: EOG signal recording was carried out on a healthy volunteer by placing the two measuring ferrimagnetic epidermal electrodes above and below the volunteer's right eye, in order to record a single vertical lead able to capture up-and-down eye movements (see Figure 4G). The ground electrode was put on the subject's forehead, between the eyes. At the same time, two Ag/AgCl electrodes were placed similarly to the ferrimagnetic ones, but slightly shifted on the right side, thus allowing to record a similar EOG vertical lead. During the acquisitions, the volunteer was asked to perform up-and-down eye movements, by directing the gaze to a top or a bottom target, respectively. Specifically, the subject was asked to stare at each target for 2 s, while maintaining a neutral eye position (i.e., looking in front of him) for about 5 s between the two saccadic movements.

After centering the biopotentials (i.e., by subtracting the offset value that was acquired during the initial neutral fixation), EOG signal quality was assessed by evaluating the normalized Pearson's correlation coefficient ρ on the full-length recording, and the consistency in the detection of saccadic movement onsets. Specifically, the ρ was computed between the EOG signal recorded by the epidermal electrodes and the simultaneous EOG signal acquired by disposable Ag/AgCl ones, as for ECG and EMG signals. Due to the low-frequency nature of this kind of biopotential, no low-frequency noise level was studied in this case. Finally, the quality of EOG signals was also appraised by comparing the onsets detected for each saccadic movement in both recordings. Indeed, the onsets of the eye saccadic movements were automatically identified by exploiting the algorithm introduced by Engbert and Mergenthaler, by imposing a minimal saccade duration equal to 6 ms and $\lambda = 5$.[53]

Supporting Information

Supporting Information is available from the Wiley Online Library or from the author.

Conflict of Interest

The authors declare no conflict of interest.

Data Availability Statement

The data that support the findings of this study are available from the corresponding author upon reasonable request.

[1] D.-H. Kim, N. Lu, R. Ma, Y.-S. Kim, R.-H. Kim, S. Wang, J. Wu, S. M. Won, H. Tao, A. Islam, K. J. Yu, T.-I. Kim, R. Chowdhury, M. Ying, L. Xu, M. Li, H.-J. Chung, H. Keum, M. McCormick, P. Liu, Y.-W. Zhang, F. G. Omenetto, Y. Huang, T. Coleman, J. A. Rogers, *Science* **2011**, *333*, 838.

[2] W. Jia, A. J. Bandodkar, G. Valdés-Ramírez, J. R. Windmiller, Z. Yang, J. Ramírez, G. Chan, J. Wang, *Anal. Chem.* **2013**, *8514*, 6553.

[3] A. J. Bandodkar, W. Jia, C. Yardımcı, X. Wang, J. Ramirez, J. Wang, *Anal. Chem.* **2014**, *871*, 394.

[4] S. Imani, A. J. Bandodkar, A. M. V. Mohan, R. Kumar, S. Yu, J. Wang, P. P. Mercier, *Nat. Commun.* **2016**, *7*, 11650.

[5] H. Lee, C. Song, Y. S. Hong, M. S. Kim, H. R. Cho, T. Kang, K. Shin, S. H. Choi, T. Hyeon, D.-H. Kim, *Sci. Adv.* **2017**, *33*, e1601314.

[6] J. Alberto, C. Leal, C. Fernandes, P. A. Lopes, H. Paisana, A. T. de Almeida, M. Tavakoli, *Sci. Rep.* **2020**, *101*, 1.

[7] S. Lee, A. Reuveny, J. Reeder, S. Lee, H. Jin, Q. Liu, T. Yokota, T. Sekitani, T. Isoyama, Y. Abe, Z. Suo, T. Someya, *Nat. Nanotechnol.* **2016**, *11*, 472.

[8] F. A. Viola, A. Spanu, P. C. Ricci, A. Bonfiglio, P. Cosseddu, *Sci. Rep.* **2018**, *8*, 8073.

[9] Y. Hattori, L. Falgout, W. Lee, S.-Y. Jung, E. Poon, J. W. Lee, I. Na, A. Geisler, D. Sadhwani, Y. Zhang, Y. Su, X. Wang, Z. Liu, J. Xia, H. Cheng, R. C. Webb, A. P. Bonifas, P. Won, J.-W. Jeong, K.-I. Jang, Y. M. Song, B. Nardone, M. Nodzenski, J. A. Fan, Y. Huang, D. P. West, A. S. Paller, M. Alam, W.-H. Yeo, J. A. Rogers, *Adv. Healthcare Mater.* **2014**, *3*, 1597.

[10] J. W. Jeong, W. H. Yeo, A. Akhtar, J. J. Norton, Y. J. Kwack, S. Li, S. Y. Jung, Y. Su, W. Lee, J. Xia, H. Cheng, *Adv. Mater.* **2013**, *2547*, 6839.

[11] L. Bareket, L. Inzelberg, D. Rand, M. David-Pur, D. Rabinovich, B. Brandes, Y. Hanein, *Sci. Rep.* **2016**, *6*, 25727.

[12] J. G. Webster, *Medical Instrumentation: Application and Design*, 4th ed., John Wiley & Sons, Hoboken, NJ **2010**.

[13] D. J. Hewson, J.-Y. Hogrel, Y. Langeron, J. Duchene, *J. Electromyogr. Kinesiol.* **2003**, *13*, 273.

[14] A. J. Casson, R. Saunders, J. C. Batchelor, *IEEE Sens. J.* **2017**, *17*, 2205.

[15] C. Wang, M. Cai, Z. Hao, S. Nie, C. Liu, H. Du, J. Wang, W. Chen, J. Song, *Adv. Intell. Syst.* **2021**, *3*, 2100031.

[16] L. Inzelberg, D. Rand, S. Steinberg, M. David-Pur, Y. Hanein, *Sci. Rep.* **2018**, *81*, 2058.

[17] A. Mascia, R. Collu, A. Spanu, M. Fraschini, M. Barbaro, P. Cosseddu, *Sensors* **2023**, *23*, 766.

[18] X. Du, W. Jiang, Y. Zhang, J. Qiu, Y. Zhao, Q. Tan, S. Qi, G. Ye, W. Zhang, N. Liu, *ACS Appl. Mater. Interfaces* **2020**, *12*, 56361.

[19] K.-I. Jang, S. Y. Han, S. Xu, K. E. Mathewson, Y. Zhang, J.-W. Jeong, G.-T. Kim, R. C. Webb, J. W. Lee, T. J. Dawidczyk, R. H. Kim, Y. M. Song, W.-H. Yeo, S. Kim, H. Cheng, S. I. Rhee, J. Chung, B. Kim, H. U. Chung, D. Lee, Y. Yang, M. Cho, J. G. Gaspar, R. Carbonari, M. Fabiani, G. Gratton, Y. Huang, J. A. Rogers, *Nat. Commun.* **2014**, *5*, 4779.

[20] Z. Jiang, Md O. G. Nayeem, K. Fukuda, S. Ding, H. Jin, T. Yokota, D. Inoue, D. Hashizume, T. Someya, *Adv. Mater.* **2019**, *31*, 1903446.

[21] L. M. Ferrari, U. Ismailov, J. M. Badier, F. Greco, E. Ismailova, *npj Flexible Electron.* **2020**, *4*, 4.

[22] M. B. Lodi, N. Curreli, A. Fanti, C. Cuccu, D. Pani, A. Sanginario, A. Spanu, P. Motto Ros, M. Crepaldi, D. Demarchi, G. Mazzarella, *IEEE Access* **2020**, *8*, 160099.

[23] A. Spanu, A. Botter, A. Zedda, G. L. Cerone, A. Bonfiglio, D. Pani, *IEEE TNSRE* **2021**, *29*, 1661.

[24] W. Jeonga, G. Gwona, J.-H. Haa, D. Kima, K.-J. EombJu, H. Parkc, S. JuKangb, B. Kwakd, J.-I. Honga, S. Leea, D. C. Hyunc, S. Leea, *Biosens. Bioelectron.* **2021**, *171*, 112717.

[25] E. Bihar, T. Roberts, M. Saadaoui, T. Hervé, J. B. De Graaf, G. G. Malliaras, *Adv. Healthcare Mater.* **2017**, *6*, 1601167.

[26] Y. Won, J. J. Lee, J. Shin, M. Lee, S. Kim, S. Gandla, *ACS Sens.* **2021**, *6*, 967.

[27] Y. Chen, G. Zhou, X. Yuan, C. Li, L. Liu, H. You, *Biosens. Bioelectron.* **2022**, *206*, 114118.

[28] L.-W. Lo, J. Zhao, H. Wan, Y. Wang, S. Chakrabartty, C. Wang, *ACS Appl. Mater. Interfaces* **2021**, *13*, 21693.

[29] Y. Wang, Z. Qu, W. Wang, D. Yu, *Colloids Surf., B* **2021**, *208*, 112088.

[30] A. Spanu, M. Taki, G. Baldazzi, A. Mascia, P. Cosseddu, D. Pani, A. Bonfiglio, *Bioengineering* **2022**, *9*, 205.

[31] L. M. Ferrari, S. Sudha, S. Tarantino, R. Esposti, F. Bolzoni, P. Cavallari, C. Cipriani, V. Mattoli, F. Greco, *Adv. Sci.* **2018**, *5*, 1700771.

[32] F. Zabihi, M. Eslamian, *J. Coat. Technol. Res.* **2015**, *12*, 711.

[33] F. Gong, C. Meng, J. He, X. Dong, *Prog. Org. Coat.* **2018**, *121*, 89.

[34] J. G. Tait, B. J. Worfolk, S. A. Maloney, T. C. Hauger, A. L. Elias, J. M. Buriak, K. D. Harris, *Sol. Energy Mater. Sol. Cells* **2013**, *110*, 98.

[35] M. G. Say, I. Sahalianov, R. Brooke, L. Migliaccio, E. D. Głowacki, M. Berggren, M. J. Donahue, I. Engquist, *Adv. Mater. Technol.* **2022**, *7*, 2101420.

[36] J. Wang, S. Lee, T. Yokota, Y. Jimbo, Y. Wang, Md O. G. Nayeem, M. Nishinaka, T. Someya, *ACS Appl. Electron. Mater.* **2020**, *2*, 3601.

[37] X. Wu, A. Surendran, M. Moser, S. Chen, B. T. Muhammad, I. P. Maria, I. McCulloch, W. L. Leong, *ACS Appl. Mater. Interfaces* **2020**, *12*, 20757.

[38] S. Taccola, T. da Veiga, J. H. Chandler, O. Cespedes, P. Valdastri, R. A. Harris, *Sci. Rep.* **2022**, *12*, 17931.

[39] C. H. Chen, A. Torrents, L. Kulinsky, R. D. Nelson, M. J. Madou, L. Valdevit, J. C. LaRue, *Synth. Met.* **2011**, *161*, 2259.

[40] A. E. Kovalev, K. Dening, B. N. Persson, S. N. Gorb, *Beilstein J. Nanotechnol.* **2014**, *5*, 1341.

[41] C. Trojahn, G. Dobos, M. Schario, L. Ludriksone, U. Blume-Peytavi, J. Kottner, *Skin Res. Technol.* **2015**, *21*, 69.

[42] P. Chavoshnejad, A. H. Foroughi, N. Dhandapani, G. K. German, M. J. Razavi, *Phys. Rev. E* **2021**, *104*, 034406.

[43] K. Articus, C. A. Brown, K. P. Wilhelm, *Skin Res. Technol.* **2001**, *7*, 164.

[44] R. Ohtsuki, T. Sakamaki, S. Tominaga, *Opt. Rev.* **2013**, *20*, 94.

[45] A. Spanu, A. Mascia, G. Baldazzi, B. Fenech-Salerno, F. Torrisi, G. Viola, A. Bonfiglio, P. Cosseddu, D. Pani, *Front. Bioeng. Biotechnol.* **2022**, *23*, 820217.

**ADVANCED
SCIENCE NEWS**

www.advancedsciencenews.com

**ADVANCED
ENGINEERING
MATERIALS**

www.aem-journal.com

[46] G. D. Clifford, F. Azuaje, P. McSharry, *Advanced Methods and Tools for ECG Data Analysis*, Artech House, Boston, FL **2006**.

[47] A. Spanu, A. Bonfiglio, D. Pani, in *42nd Annual Int. Conf. IEEE Engineering in Medicine & Biology Society (EMBC)*, IEEE, Piscataway, NJ **2020**.

[48] S. Ryf, T. Wolber, F. Duru, R. Luechinger, *Technol. Health Care* **2008**, *16*, 13.

[49] C. A. Finch, *Chemistry and Technology of Water-Soluble Polymers*, Springer, Boston, MA **1983**, https://doi.org/10.1007/978-1-4757-9661-2_17.

[50] P. Kligfield, L. S. Gettes, J. J. Bailey, R. Childers, B. J. Deal, E. W. Hancock, G. van Herpen, J. A. Kors, P. Macfarlane, D. M. Mirvis, O. Pahlm, P. Rautaharju, G. S. Wagner, *J. Am. Coll. Cardiol.* **2007**, *49*, 1109.

[51] J. P. Martínez, R. Almeida, S. Olmos, A. P. Rocha, P. Laguna, *IEEE TBE* **2004**, *51*, 4.

[52] C. J. De Luca, L. Donald Gilmore, M. Kuznetsov, S. H. Roy, *J. Biomech.* **2010**, *43*, 1573.

[53] R. Engbert, K. Mergenthaler, *Proc. Natl. Acad. Sci. U. S. A.* **2006**, *103*, 71927.